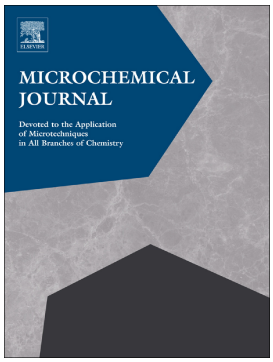

Improving reproducibility between batches of silver nanoparticles using an experimental design approach

Rodrigo Nicolás Núñez, Alicia Viviana Veglia, Natalia Lorena Pacioni

PII: S0026-265X(18)30315-1
DOI: doi:10.1016/j.microc.2018.05.017
Reference: MICROC 3165

To appear in: *Microchemical Journal*

Received date: 14 March 2018
Revised date: 18 April 2018
Accepted date: 11 May 2018

Please cite this article as: Rodrigo Nicolás Núñez, Alicia Viviana Veglia, Natalia Lorena Pacioni , Improving reproducibility between batches of silver nanoparticles using an experimental design approach. The address for the corresponding author was captured as affiliation for all authors. Please check if appropriate. Microc(2017), doi:10.1016/j.microc.2018.05.017

Improving reproducibility between batches of silver nanoparticles using an experimental design approach.

Rodrigo Nicolás Núñez[1,2], Alicia Viviana Veglia[1,2] and Natalia Lorena Pacioni[1,2]*

[1]*Universidad Nacional de Córdoba, Facultad de Ciencias Químicas, Departamento de Química Orgánica. Haya de la Torre y Medina Allende s/n, X5000HUA, Ciudad Universitaria, Córdoba, Argentina.*

[2]*Consejo Nacional de Investigaciones Científicas y Técnicas (CONICET), INFIQC, Córdoba, Argentina.*

Phone: +54-351-5353867

Emails: rnunez@fcq.unc.edu.ar; aveglia@fcq.unc.edu.ar

Corresponding author*: nataliap@fcq.unc.edu.ar*

Abstract

An optimized method for the synthesis of silver nanoparticles (AgNP) using gallic acid as reductant was achieved using design of experiment strategies based on response surface methodologies. Fractional factorial design was used in the screening stage, the Box-Behnken method was employed to model the target responses and finally, the optimization step was done using Desirability function. The obtained AgNP presented improved repetitivity and reproducibility of photophysical properties between batches compared to the synthesis method reported in literature. Intra-assays, intermediate precision and reproducibility tests were performed and proved the different AgNP batches presented equal optical responses, average size and size distribution at a 95% confidence level. In addition, a test on shelf life estimated the optimized AgNP preserve their properties at least for 38 days and especially, zeta potential measurements indicated their low tendency to flocculation as long as 120 days. Furthermore, a remarkable improvement in obtaining reproducible Stern-Volmer constants in fluorescence quenching experiments using Carbazole as fluorophore was observed compared to nanoparticles synthesized by a non-optimal method.

Keywords

Silver nanoparticles synthesis; Gallic acid; Fractional Factorial Design, Box-Behnken; Fluorescence quenching; Response surface models

1. Introduction

It is already well-established that properties of nanomaterials are highly dependent on size, which is usually reported as the average diameter (for spheres) obtained from the nanoparticle size histogram distribution [1]. However, obtaining identical batches for manufactured nanoparticles (especially metallic) is often a difficult task, indeed at laboratory scale. Differences between batches will impact on determining accurately and precisely properties associated to nanoparticles, for example, analysis of their interaction with other molecules [2].

Currently, silver nanoparticles (AgNP) are among the most employed metal nanoparticles due to their unique and multifunctional properties, making them able to be employed in diverse applications such as catalysis [3], plasmonics [4–6], ink-jet printing [7], biomaterials [8,9] and sensing [10]. Despite the many uses AgNP have, obtaining reproducible results for different batches is hard, when variations in nanoparticle features affect their performance.

Generally, AgNP for research purposes are often synthesized in the lab bench using different methodologies like chemical reduction, photochemical and sonochemical methods among others synthetic alternatives [11]. The outcome of the synthesis by chemical reduction, one the most frequently used methods, is highly dependent on the identity of reactants as well as the concentration, time of reaction and temperature [11–13]. Hence, establishing the optimal conditions that can render a product preserving its main physicochemical characteristics from batch to batch is still a challenge.

Among other chemical methods, reduction of Ag^+ by gallic acid (GA, Scheme 1) presents a simple synthetic alternative to obtain AgNP using a biocompatible molecule, mild reaction conditions (room temperature, water) and relatively short times (30 min) [14]. Nevertheless, using those reported experimental conditions, the resulting AgNP size distributions are usually different from batch to batch: ~32 nm in the original article [14], ~5 and ~29 nm in our previous work [15]; or using slightly modified procedures size distributions are also variable: ~7 nm [16], ~29 nm [16] and 14 nm [17].

INSERT SCHEME 1

Design of experiments (DoE) employing response surface methodologies (RSM) [18,19] has been proved to provide understanding of the interacting factors and their optimization during the synthesis of nanomaterials [20–25]. For instance, Domingos *et al*. [21,22] used DoE for choosing the best polymer frameworks based on dextran or polyethyleneimine to obtain highly catalytically active AgNP; Lim *et al.* [24] analyzed the interactions between different experimental factors for the synthesis of AgNP using ascorbic acid as reducing agent; and Liu *et al.* [25] optimized a synthetic procedure for obtaining Ag-Cu bimetallic nanoparticles. However, none of them focused on increasing reproducibility between batches.

In this work, we present a synthetic strategy to obtain reproducible batches of silver nanoparticles synthesized by chemical reduction using gallic acid ($AgNP_g$) based on a DoE methodology. First, at the screening stage we used a Fractional Factorial Design (FFD) [18,26,27] to find out the significant factors affecting the $AgNP_g$ outcome, then at the modeling step we employed a Box-Behnken design (BBD) [27–29] to model the second-order response surface, and finally we used the Desirability function [27,30,31] for the multiple responses optimization. In addition to statistical analysis for intra-assays, intermediate precision and reproducibility, we also evaluated the shelf-life and stability of the synthesized $AgNP_g$ under the optimized experimental conditions. Furthermore, we compared how the reproducibility between batches impacts on the analysis of Carbazole fluorescence quenching by $AgNP_g$. The optimized method presented a relevant improvement in reproducibility respect to the original procedure.

2. Materials and methods

2.1. Reactants. Monohydrate gallic acid (GA) and sodium hydroxide were Merck, $AgNO_3$ (BioPack) and Carbazole 98% (Sigma). All reactants were used as received. Water was MilliQ quality obtained from a Millipore instrument (resistivity, 25ºC: 18 MΩ cm^{-1}).

2.2. Instrumentation. All absorption spectra were measured in a UV–vis Shimadzu 1800 spectrophotometer in the 200–800 nm wavelength range using quartz cells (1 cm path-length).

Fluorescence measurements were done using a Cary Eclipse fluorescence spectrophotometer (Agilent) with a Peltier temperature controller set at 25,0 ºC. Transmission Electron Microscopy images were obtained using a TEM-Jeol 1120 electron microscope, 80 kV accelerating voltage on Carbon-coated copper grids (300 mesh, Electron Microscopy). Zeta potential and polydispersity index using Dynamic Light Scattering (DLS) were measured in a Delsa^{TM} Nano S Particle Analyzer (Beckman Coulter) at room temperature. Centrifugation was performed in an Eppendorf Centrifuge 5804.

Data analysis was done using Design Expert 10® or Minitab Inc.® software, and all graphs were plotted using Origin 8.0®.

2.3. Experimental design for the synthesis of $AgNP_g$

Based on the synthetic procedure reported by Yoosaf *et al.* [14] (10 μM GA, 74μM $AgNO_3$, 740 μM NaOH, stirring 30 min at room temperature in the dark), we decided to employ a two-level fractional factorial design (FFD) in order to identify which preparation factors (NaOH, gallic acid and $AgNO_3$ concentrations, reaction time and stirring speed) are the most critical by having a significant effect on the selected response (ψ, eq. 1). In equation 1, A_{max}, λ_{max} and FWHM are the maximum absorbance, the maximum wavelength and full width at half maximum at the surface plasmon resonance band (SPR), respectively. These parameters are related to the concentration of AgNP, the size and the polydispersity, correspondingly [21].

$$\psi = \frac{A_{max}}{\lambda_{max}\, FWHM} \qquad \text{eq.1}$$

Fractional Factorial Designs (FFD) are a first-order response surface model to explore the effects of controllable factors on a response of interest. They use known properties of the design to selectively reduce the size of an experiment while holding critical information [19,26]. One of the most popular FFD is the two-level FFD, where each factor is evaluated at two levels coded as +1 (the highest value) and -1 (the lowest value). The chosen design consists of $2^{(k-p)}$ experiments, where k is the number of

factors and p is the number of design generators. For the synthesis of $AgNP_g$, k is 5 ([NaOH], [$AgNO_3$], [GA], reaction time and stirring speed) and p is 1 with the defining relation *I=ABCDE,* then the resulting FFD is one-half fraction of resolution V, a screening design to estimate the main effects and two-factor interactions provided that all the three-factor and higher interactions are negligible [18].

Table 1. Factors and coded levels considered for the 2_V^{5-1} design run with two replicates (I and II). Experimental matrix and obtained responses.

Factor		Symbol	Low level (-1)	Central point		High level (+1)	
[NaOH] (μM)		A	500	750		1000	
[$AgNO_3$] (μM)		B	50	75		100	
[GA] (μM)		C	5	12.5		20	
time (min)		D	10	30		50	
stirring speed		E	1	5.5		10	
Standard	**Run**	**A**	**B**	**C**	**D**	**E**	**ψ (10^{-8} nm^{-2})**
							I **II**
1	5	-	-	-	-	-	60.1 66.2
2	20	+	-	-	-	+	64.3 75.1
3	14	-	-	+	-	+	151.8 146.9
4	10	+	-	+	-	-	153.7 149.6
5	4	-	+	-	-	+	113.2 118.5
6	12	+	+	-	-	-	109.6 113.9
7	18	-	+	+	-	-	246.9 231.8
8	3	+	+	+	-	+	259.8 240.9
9	15	-	-	-	+	-	196.2 182.7
10	9	+	-	-	+	+	190.6 203.1
11	6	-	-	+	+	+	276.9 289.6
12	16	+	-	+	+	-	255.4 276.6
13	21	-	+	-	+	+	175.3 181.3
14	1	+	+	-	+	-	169.8 159.6
15	2	-	+	+	+	-	336.0 343.5
16	17	+	+	+	+	+	386.1 345.7
17	7	0	0	0	0	0	153.0 146.7
18	19	0	0	0	0	0	143.5 126.3
19	11	0	0	0	0	0	171.1 162.4
20	8	0	0	0	0	0	136.6 148.1
21	13	0	0	0	0	0	156.6 143.4
22	22	0	0	0	0	0	139.6 120.3

Thus, each factor was employed at two levels, -1 and +1, plus a central point. This design involved 32 experiments plus twelve central points in order to evaluate the linear effects and the

curvature of the variables (Table 1). Experiments were randomized to avoid systematic errors. The evaluation of the results of the FFD was carried out using analysis of variance (ANOVA) at the 95% confidence level, and graphical analysis using the Pareto chart (Fig. 1) and the half-normal probability plot (not shown).

Once the principal factors were determined, the multivariate optimization was continued based on a second-order response surface model employing a BBD (Table 2). Briefly, BBDs are a class of spherical, rotatable designs (or nearly rotatable) based on three-level incomplete factorial designs employed to obtain second-order relationships between factors and responses [29]. The number of experiments involved in a BBD is defined as $N = 2k(k-1) + C_0$, where k is number of factors and C_0 is the number of central points [29]. Then, the BBD comprised 17 experiments where the selected target functions were A_{max}, λ_{max} and FWHM (Table 3). Using ANOVA, principal factors, interaction factors and second-order terms were determined.

Table 2. Factors and coded levels employed for the BBD in this work

Symbol	Factor	Low level (-)	Central point (0)	High level (+)
B	[$AgNO_3$] (μM)	20	110	200
C	[GA] (μM)	5	27.5	50
D	time (min)	5	27.5	50

2.3.1. Desirability function

Briefly, using the statistical program each response was transformed into a particular desirability function that varies from 0 (non-desirable) to 1 (totally desirable), and the desirability profiles were obtained. By means of inspecting these profiles, the optimal responses were associated to a set of experimental conditions (optimal level for each factor).

2.4. Optimization of post-synthesis protocol. Commonly, to clean-up and concentrate the $AgNP_g$ the technique used is centrifugation. In order to evaluate if the centrifugation rate has some effect on the selected response ψ we decided to optimize this parameter. Using a univariate design, eight experiments were performed employing the experimental conditions obtained by BBD to analyze the centrifugation speed effect in the range 1000 to 8000 rpm. Once optimized, a prediction test was done using six samples centrifuged at 8000 rpm.

Table 3. Box-Behnken experimental matrix and obtained results

		Factors			Responses		
Standard	**Run**	**B**	**C**	**D**	**A_{max}/a.u.**	**λ_{max}/nm**	**FWHM/nm**
1	16	-	-	0	0.016	405.5	74.5
2	5	+	-	0	0.030	391.5	70.0
3	9	-	+	0	0.031	413.0	94.5
4	14	+	+	0	0.159	397.0	66.0
5	17	-	0	-	0.021	406.5	79.0
6	15	+	0	-	0.166	393.5	58.5
7	6	-	0	+	0.023	420.5	96.0
8	12	+	0	+	0.149	396.0	60.5
9	8	0	-	-	0.042	396.0	68.0
10	7	0	+	-	0.086	401.5	75.0
11	1	0	-	+	0.042	397.5	68.5
12	13	0	+	+	0.090	400.5	71.5
13	2 (C)	0	0	0	0.082	399.5	71.0
14	3 (C)	0	0	0	0.084	402.0	74.0
15	11 (C)	0	0	0	0.085	399.0	72.5
16	10 (C)	0	0	0	0.089	400.5	70.5
17	4 (C)	0	0	0	0.080	400.0	71.5

(C) Central Point

2.5. Quenching experiments. Solutions of carbazole (100 nM) in 95% v/v phosphate buffer pH 6.94 0.05 M and 2% v/v methanol were excited at 290.0 nm using 5.0 nm slit widths in the absence and presence of $AgNP_g$ at different concentrations. All spectra were recorded in the 330.0-450.0 nm range at 25.0 ºC in quartz cells 1.0 cm path length. Spectra were corrected for inner filter effect using equation 2 [32,33].

$$F_{corr}=F_{obs}\times\left(\frac{2.3S_2A^{ex}}{1-10^{-S_2A^{ex}}}\times 10^{-S_3A^{em}}\times\frac{2.3S_1A^{em}}{1-10^{-S_1A^{em}}}\right) \quad \text{eq. 2}$$

where, F_{corr} and F_{obs} are the corrected and observed emission fluorescence intensity, respectively, S_1 (0.8 cm), S_2 (1.0 cm) and S_3 (0.5 cm) are cuvettes dimensions as described in [32,34], A^{ex} and A^{em} are the absorbances/cm at the excitation and emission wavelengths, correspondingly.

Both, $AgNP_g$ synthesized using the literature method and $AgNP_g^{opt}$ obtained using the optimized conditions presented in this work were employed.

3. Results and Discussion

3.1. Multivariate optimization for $AgNP_g$ synthesis

First, we chose to evaluate using a 2_V^{5-1} FFD which of the following factors: [NaOH], [GA], [$AgNO_3$], reaction time and stirring speed, affect significantly the selected response ψ (eq. 1) in order to get $AgNP_g$ in high yield, more monodisperse and keeping a constant average size between batches. The main effects and two-level factor interactions were determined using Analysis of Variance (ANOVA, Table S1 in the Supplementary material) resulting significant at a 95% confidence level ($p<0.05$) the following main factors: [$AgNO_3$], [GA] and time, and the two-factor interaction [NaOH] × stirring speed. These results were better visualized in the Pareto chart (Fig. 1) where the vertical line indicates the critical *t*-value (t: 2.059), and the horizontal bars correspond to the t-Student test for each analyzed effect. Similar conclusion was reached from the half normal probability plot (not shown). However, a Lack of Fit (LOF) was detected for this first-order model on the response in agreement with the presence of curvature (quadratic effect) [19]. For this reason, we proceeded to employ a second-order RSM based on a BBD design (Table 3) to assess the mathematical function that models the target spectroscopic responses (A_{max}, λ_{max} and FWHM) as a function of main factors {[$AgNO_3$] (B), [GA] (C) and reaction time (D)}. In order to fix the levels of the interacting factors ([NaOH] × stirring speed) in

our BBD, we built up the interaction plot (Fig S1 in the Supplementary material). Then, we chose as optimal the combination used as central point (740 μM in NaOH and stirring rate of 5.5), though giving a lower response mean, may provide more precise results considering the lower range (max - min) for Ψ (≈50, Table 1) than working at extreme conditions (≈300, Table 1) [19].

INSERT FIG. 1

A multiple regression fit for each target response was obtained by minimum squared methodology. The statistical validity of the fitted model (second-order polynomial) was achieved using the ANOVA test in order to determine the significant terms and the p-values for LOF. Table 4 summarizes these results together with the values of R-Squared (R^2), adjusted R-Squared (R^2_{adj}) and predicted R-Squared (R^2_{pred}).

Table 4. Significant terms and statistics summary of RSM for $AgNP_g$ synthesis optimization

	Term	***R^2***	***R^2_{adj}***	***R^2_{pred}***	***LOF***	***Fitted model***
A_{max}	B, C, D, BC, BD, C^2, D^2	0.9928	0.9856	0.8963	0.0714	$A_{max}=-1.76\times10^{-3} + 2.20\times10^{-4}$ B + 2.77×10^{-3} C – 1.02×10^{-3} D + 2.2×10^{-5} BC - 8×10^{-6} BD – 7.6×10^{-5} C^2 + 3.8×10^{-5} D^2
λ_{max} (nm)	B, C	0.9123	0.8976	0.8578	0.3936	λ_{max} = 404.9 – 0.067 B + 0.092 C
FWHM (nm)	B, C, D, BC, BD, C^2, D^2	0.9655	0.9311	0.8173	0.4632	FWHM (nm)= 73.3 – 0.0478 B + 0.0305 C + 0.317 D – 2.5×10^{-3} BC + 1.17×10^{-3} BD + 6.69×10^{-3} C^2 – 8.95×10^{-3} D^2

Both A_{max} and FWHM are modelled using the same significant terms including linear, quadratic and interaction terms (Table 4); whereas only the linear contributions of [$AgNO_3$] and [GA] affect λ_{max}.

For all the examined responses, the p-value for LOF was not significant ($p > 0.05$) indicating the fitted models are adequate. The fitted model for A_{max} explains the data variability in a 98.56% ($R^2_{adj} = 0.9856$) and it is able to predict 89.63% of future data variability ($R^2_{pred} = 0.8963$), demonstrating satisfactorily the reliability of the results. In the case of FWHM, 93.11% of data variability ($R^2_{adj} = 0.9311$) and 81.73% of future data variability are acceptable explained by the model, while the modelled λ_{max} explicates 89.76% ($R^2_{adj} = 0.8976$) of data variability and 81.73% of future data variability ($R^2_{pred} = 0.8173$). For all the cases there is a good agreement between R^2_{adj} and R^2_{pred} as they differ in less than 0.2 [35,36]. In addition, diagnosis graphs (not shown) like the normal probability distributions, residuals vs. predicted, and Cook distance were evaluated demonstrating the results are reasonably explained by the model.

The response surfaces built up using equations presented in Table 4 are shown in Figs. 2-4. Each 3D graph shows a target response as a function of two factors and the shape reflects the interactions and curvatures for the variables when corresponding. Figs. 2A-C represent A_{max} versus [$AgNO_3$] and [GA], against [$AgNO_3$] and reaction time, and versus reaction time and [GA], respectively. It can be observed that generally, A_{max} increases with increasing concentrations of Ag^+ (Figs. 2A and B) which it is expected as A_{max} is related to $AgNP_g$ yield, and this yield would depend on the silver precursor amount. In addition, it is visible the quadratic dependence on [GA] and reaction time (Fig. 2C).

INSERT FIG. 2

Figs. 3A-C show the variation of λ_{max} with [$AgNO_3$] and [GA], with [$AgNO_3$] and time, and with [GA] and time, respectively. Interestingly, the maximum SPR wavelength (a parameter closely associated to size) red-shifts when [GA] increases or [$AgNO_3$] decreases clearly observed in Fig. 3A. This mainly reflects size will be larger at low concentrations of $AgNO_3$. On the other hand, reaction time does not influence significantly the position of λ_{max} (Figs. 3B and 3C).

INSERT FIG 3

Regarding the FWHM, a parameter related to polydispersity (the narrower the SPR band the more monodisperse the nanoparticles), Figs. 4A-C expose the surface response profiles obtained with [$AgNO_3$] and [GA], [$AgNO_3$] and reaction time, and [GA] and reaction time, correspondingly. It can be observed that smaller FWHM are obtained with high [$AgNO_3$] and low [GA] (Fig. 4A), which indicates this combination can lead to more monodisperse samples. Again, a curvature is evident for variables reaction time and [GA] (Fig. 4C).

INSERT FIG. 4

3.1.1 Optimal conditions for $AgNP_g$

In a multiple response optimization, Desirability Function (DF) method proposed by Derringer and Suich [30] is one of the most popular chemometrics tools used to find the experimental conditions to reach simultaneously the optimal value for all the evaluated factors [27]. DF always takes values between 0 (the unfavorable response) and 1 (the ideal response). In this work, we aimed to obtain $AgNP_g$ with the smaller average diameter, monodisperse and in high yield. Then, desirability 1 was assigned to the largest response obtained in the BBD (Table 3) for A_{max} and the smallest response for λ_{max} and FWHM, and vice versa for desirability 0. In order to reach this goal, each response was maximized or minimized accordingly, with a +++ (3 of 5) significance. Then, the optimal solution presented a desirability value of 0.959 (Table 5).

Table 5. Constraints of factors[a] and responses for optimization and obtained solution using DF.

Constraints				
Name	**Goal**	**Lower limit**	**Upper limit**	**Importance**
$[AgNO_3]$/ μM	Is in range	20	200	3
[GA]/ μM	Is in range	5	50	3
Reaction time/ min	Is in range	5	50	3
A_{max}	Maximize	0.016	0.167	3
λ_{max}/nm	Minimize	393.5	406.5	3
FWHM/nm	Minimize	58.5	96.0	3
Solution				
$[AgNO_3]$/ μM	**[GA]/ μM**	**Reaction time/ min**	**Desirability**	
200	27.25	5	0.959	

[a]Non significant factors were kept at the literature level, [NaOH]: 740 μM and stirring rate 5.5.

Finally, we predicted the values that the different responses can take at the optimal factors combinations (Table 5) using the fitted models (Table 4). To verify the predictions, we did the $AgNP_g$ synthesis using this optimal condition (6 replicates) and compared with the predicted value, determining the great agreement between predicted and experimental data within the 95% confidence prediction interval (PI) (Table 6).

Table 6. Prediction test for the optimization

Response	**Predicted value**	**SD[a]**	**n**	**Experimental mean ($\bar{x}$)**	**95% confidence PI**
A_{max}	0.167	0.006	6	0.16	$0.150 < \bar{x} < 0.180$
λ_{max} / nm	394	1	6	395	$392 < \bar{x} < 396$
FWHM/ nm	58	1	6	61.5	$54.9 < \bar{x} < 62.1$

[a]SD: standard deviation.

3.2. Centrifugation optimization

Besides finding the optimal synthesis conditions that lead to the desired $AgNP_g$, the post-synthesis protocol, for example centrifugation, is also a relevant step. The clean-up procedure is usually performed to pre-concentrate the stock nanoparticles in addition to eliminate unreacted precursors and excess of stabilizers. In our case, we have chosen as post-synthesis treatment centrifugation. As our final goal was to improve reproducibility between batches, we decided to evaluate separately how the centrifugation rate affected the response ψ (Eq. 1). In this case, a univariate design was employed and analyzed using ANOVA. The fitted model (Eq. 3) corresponds to a second-order polynomial where both quadratic (p: 0.0049) and linear ($p<0.0001$) contributions were significant at a 95% confidence. A p-value for LOF of 0.9111 indicates the adequacy of the fit together with the regression coefficients (R^2_{Adj} >0.964 and R^2_{pred}>0.920) denoting that 96.4% of the data variability and 92% of future data variability, respectively are explained by the model. In equation 3, x is the centrifugation rate in revolutions per minute (rpm). According to this model, increasing the centrifugation rate will maximize the response, so the limit is defined by design space . In our case, this corresponded to 8000 rpm. Again, the prediction capacity was also evaluated by comparing the predicted value against the experimental mean from 6 replicates at the optimum condition. The obtained experimental response (100×10^{-7}) was compared to the predicted one (103×10^{-7}) indicating the validity of the quadratic model at the 95% confidence.

$$\psi(10^{-6}nm^{-2}) = 1.19 - 7.8\times10^{-4}x + 2.4\times10^{-7}x^2 \qquad \text{eq. 3}$$

3.3. Performance of the optimized method

Intra-assays precision (repetitivity) was determined by analyzing 10 replicates performed by the same operator under identical conditions in one day. Variation coefficient (CV%) obtained after evaluating the ψ response was 2%. Fig. 5 shows a comparison between the absorption spectra measured for $AgNP_g$ synthesized using the optimized method ($AgNP_g^{opt}$) and those $AgNP_g$ achieved under non-

optimal conditions (CV%= 23.2). In addition, intermediate precision was determined by analyzing 10 replicates of $AgNP_g^{opt}$ obtained by the same operator under identical conditions in three different days. The ANOVA result indicated there are not significant differences between the responses obtained in different days (p=0.438). A reproducibility essay was also performed using samples (n=4) synthesized using different stock reactants solutions, glassware and two different operators in different days. Again, the ANOVA test suggested there were not significant differences between the spectroscopical responses (p=0.598).

INSERT FIG. 5

In addition, we determined the average size for four $AgNP_g^{opt}$ batches using the histograms (Fig. 6) built up from TEM images. In order to corroborate the mean diameters are equal at a 0.05 significance, we performed a multiple comparison using the Games-Howell method (Fig. S2 in the Supplementary material). As all the intervals contained zero, then we can establish the means are equal [37]. Also, the polydispersity index (PDI) was determined from DLS measurements of four batches obtaining an average PDI of 0.243, which indicates monodispersity is reasonably as usually, a PDI of 0.2 represents a monodisperse sample [38].

INSERT FIG. 6

Using three independent batches we ran a test to estimate the $AgNP_g^{opt}$ shelf life before the response decreases a 20%. The response ψ was monitored for each batch for 25 days, allowing as to estimate a shelf life time around 38 days (Fig. S3 in the Supplementary material). Furthermore, the zeta potential for these batches after 120 days was in average -25 mV, indicating even after long periods of time these nanoparticles have low tendency to flocculation [39].

3.4. Batches reproducibility in quenching experiments

Once the performance of the optimized synthesis method was established, and we have proven it represented improvements in precision in a manner that different batches presented equal $AgNP_g$ characteristics, we were interested in evaluating if this enhancement will also impact in $AgNP_g$ applications. To evaluate that, we determined the Stern-Volmer constants (K_{SV}, eq. 4) for the quenching of a fluorophore, Carbazole (CZL) using three batches of $AgNP_g^{opt}$ and three batches of $AgNP_g$ obtained as in literature [14]. First, we assumed no differences between batches within each method exist, so solutions of CZL in presence of the quencher were prepared using the same volumes of AgNP. Then, the mean sizes for each batch were determined using TEM data and the respective concentrations calculated according to previous works [15,40]. Finally, the Stern-Volmer graphs were plotted using the actual concentration in AgNP (Fig. S4 in the Supplementary material), and the K_{SV} values obtained using eq. 4. Table 7 summarizes these results, and it can be observed the remarkable reproducibility for K_{SV} obtained using the $AgNP_g^{opt}$ against those produced using the non-optimal conditions.

$$\frac{F_0}{F} = 1 + K_{SV}[AgNP] \qquad \text{eq. 4}$$

Table 7. Stern-Volmer constants determined for the quenching of CZL by $AgNP_g$

	Batch #	[a]Mean size/ nm	$K_{SV}/10^9 M^{-1}$	[b]CV% (n=3)
$AgNP_g^{opt}$	1	16 (6)	3.7	1.6
	2	16 (5)	3.8	
	3	16 (6)	3.7	
$AgNP_g$	1	21 (6)	1.30	>100
	2	21 (6)	0.99	
	3[c]	20 (5) 81%; 54 (14) 19%	57.0	

[a]Standard deviation is in parenthesis. [b]Variation coefficient for the K_{SV}. [c]Batch contained two populations of two sizes.

4. Conclusions

A systematic design of experiment approach using response surface methodologies permitted finding the optimal conditions to obtain $AgNP_g$ with repetitive and reproducible properties between batches (spectroscopical characteristics, size, dispersity index, zeta potential). Furthermore, a remarkably reproducibility in $AgNP_g^{opt}$ application to determine Stern-Volmer constants showed the optimized synthesis method renders an important improvement respect to the non-optimal method. The better reproducibility between batches is likely to impact on minimizing characterization times of these silver nanoparticles (e.g. avoiding TEM) and in consequence allowing their application right after the synthesis.

Acknowledgments

This research was supported in part by grants from the ANPCyT, the SECYT-UNC, the CONICET and the MINCyT-Cordoba. We thank to Dr. Claudia Nome and Dr. Valeria Quevedo (CIAP-INTA) for technical assistance with the microscopy measurements. R.N.N is a grateful recipient of a graduated fellowships from CONICET. A.V.V. and N.L.P are research members of the CONICET of Argentine.

Appendix. Supplementary material

Supplementary information associated with this article can be found, in the online version, at (insert web address).

5. References

[1] Hornyak, Gabor L., Dutta, Joydeep, Tibbals Harry F., Rao, Anil K., Introduction to Nanoscience, CRC Press, Boca Raton, 2008.

[2] Ahumada, Manuel, Lissi, Eduardo, Montagut, Ana María, Valenzuela-Henríquez, Francisco, Pacioni, Natalia L., Alarcón, Emilio I., Association models for binding of molecules to nanostructures, Analyst. 142 (2017) 2067–2089.

[3] C. Crites, G. Hallett-Tapley, M. Frenette, M. González-Béjar, J. Netto-Ferreira, J. Scaiano, Insights into the Mechanism of Cumene Peroxidation Using Supported Gold and Silver Nanoparticles, ACS Catal. 3 (2013) 2062–2071. doi:10.1021/cs400337w.

[4] K. Stamplecoskie, C. Fasciani, J. Scaiano, Dual-Stage Lithography from a Light-Driven, Plasmon-Assisted Process: A Hierarchical Approach to Subwavelength Features, Langmuir. 28 (2012) 10957–10961.

[5] J. Scaiano, K. Stamplecoskie, Can Surface Plasmon Fields Provide a New Way to Photosensitize Organic Photoreactions? From Designer Nanoparticles to Custom Applications, J Phys Chem Lett. 4 (2013) 1177–1187.

[6] R. Gill, L. Tian, W. Somerville, E. Ru, H. Amerongen, V. Subramaniam, Silver Nanoparticle Aggregates as Highly Efficient Plasmonic Antennas for Fluorescence Enhancement, J Phys Chem C. 116 (2012) 16687–16693.

[7] A. Chiolerio, K. Rajan, I. Roppolo, A. Chiappone, S. Bocchini, D. Perrone, Silver nanoparticle ink technology: state of the art, Nanotechnol. Sci. Appl. (2016) 1. doi:10.2147/NSA.

[8] E. Alarcon, B. Vulesevic, A. Argawal, A. Ross, P. Bejjani, J. Podrebarac, R. Ravichandran, J. Phopase, E. Suuronen, M. Griffith, Coloured cornea replacements with anti-infective properties: expanding the safe use of silver nanoparticles in regenerative medicine, Nanoscale. 8 (2016) 6484–6489. doi:10.1039/C6NR01339B.

[9] S. Mclaughlin, J. Podrebarac, M. Ruel, E. Suuronen, B. Mcneill, E. Alarcon, Nano-Engineered Biomaterials for Tissue Regeneration: What Has Been Achieved So Far?, Front. Mater. 3 (2016) 67435. doi:10.3389/fmats.2016.00027.

[10] C. Wang, M. Luconi, A. Masi, L. Fernandez, Silver nanoparticles as optical sensors, in: Pozo Pérez, David (Ed.), Silver Nanoparticles, InTech, 2010: pp. 225–256.

[11] N. L. Pacioni, C. D. Borsarelli, V. Rey, A. V. Veglia, Synthetic routes for the preparation of silver nanoparticles. A mechanistic perspective., in: E. I. Alarcón, M. Griffith, K. I. Udekwu (Eds.), Silver Nanoparticles Appl., Springer, Switzerland, 2015: pp. 13–46.

[12] M. Rycenga, C. Cobley, J. Zeng, W. Li, C. Moran, Q. Zhang, D. Qin, Y. Xia, Controlling the synthesis and assembly of silver nanostructures for plasmonic applications, Chem. Rev. 111 (2011) 3669–712. doi:10.1021/cr100275d.

[13] Y. Sun, Controlled synthesis of colloidal silver nanoparticles in organic solutions: empirical rules for nucleation engineering, Chem Soc Rev. 42 (2013) 2497–2511. doi:10.1039/C2CS35289C.

[14] K. Yoosaf, B. Ipe, C. Suresh, K. Thomas, In Situ Synthesis of Metal Nanoparticles and Selective Naked-Eye Detection of Lead Ions from Aqueous Media, J. Phys. Chem. C. 111 (2007) 12839–12847.

[15] N.L. Pacioni, A.V. Veglia, Analytical strategy to detect metal nanoparticles in mixtures without previous separation, Sens. Actuators B Chem. 228 (2016) 557–564. doi:10.1016/j.snb.2016.01.064.

[16] F. Martinez-Gutierrez, P. Olive, A. Banuelos, E. Orrantia, N. Nino, E. Sanchez, F. Ruiz, H. Bach, Y. Av-Gay, Synthesis, characterization, and evaluation of antimicrobial and cytotoxic effect of silver and titanium nanoparticles, Nanomedicine Nanotechnol. Biol. Med. 6 (2010) 681–688. doi:10.1016/j.nano.2010.02.001.

[17] J. Park, S. Cha, S. Cho, Y. Park, Green synthesis of gold and silver nanoparticles using gallic acid: catalytic activity and conversion yield toward the 4-nitrophenol reduction reaction, J. Nanoparticle Res. 18 (2016) 13. doi:10.1007/s11051-016-3466-2.

[18] Douglas C. Montgomery, Design and analysis of experiments, 3rd ed., John Wiley & Sons, Ltd., Singapore, 1991.

[19] W.P. Gardiner, G. Gettinby, Experimental design techniques in statistical practice. A practical software based approach., Horwood Publishing Ltd., Chichester, 1998.

[20] C. Vasti, V. Pfaffen, E. Ambroggio, M. Galiano, R. Rojas, C. Giacomelli, A systematic approach to the synthesis of LDH nanoparticles by response surface methodology, Appl. Clay Sci. 137 (2017) 151–159. doi:10.1016/j.clay.2016.12.023.

[21] R. Eising, A. Signori, S. Fort, J. Domingos, Development of catalytically active silver colloid nanoparticles stabilized by dextran, Langmuir. 27 (2011) 11860–6. doi:10.1021/la2029164.

[22] A. Signori, K. Santos, R. Eising, B. Albuquerque, F. Giacomelli, J. Domingos, Formation of Catalytic Silver Nanoparticles Supported on Branched Polyethyleneimine Derivatives, Langmuir. 26 (2010) 17772–17779. doi:10.1021/la103408s.

[23] H. Wang, C. Wu, C. Chung, M. Lai, T. Chung, Analysis of Parameters and Interaction between Parameters in Preparation of Uniform Silicon Dioxide Nanoparticles Using Response Surface Methodology, Ind Eng Chem Res. 45 (2006) 8043–8048.

[24] J. Lim, J. Lee, A statistical design and analysis illustrating the interactions between key experimental factors for the synthesis of silver nanoparticles, Colloids Surf. Physicochem. Eng. Asp. 322 (2008) 155–163. doi:10.1016/j.colsurfa.2008.03.014.

[25] X. Liu, W. Liu, C. Wang, Z. Zheng, Optimization and modeling for one-step synthesis process of Ag–Cu nano-particles using DOE methodology, J. Mater. Sci. Mater. Electron. 27 (2016) 4265–4274. doi:10.1007/s10854-016-4292-0.

[26] R. Gunst, R. Mason, Fractional factorial design, WIREs Comput. Stat. 1 (2009) 234–244.

[27] L. Vera Candioti, M. De Zan, M. Cámara, H. Goicoechea, Experimental design and multiple response optimization. Using the desirability function in analytical methods development, Talanta. 124 (2014) 123–138. doi:10.1016/j.talanta.2014.01.034.

[28] G. Box, D. Behnken, Some New Three Level Designs for the Study of Quantitative Variables, Technometrics. 2 (1960) 455–475.

[29] S. Ferreira, R. Bruns, H. Ferreira, G. Matos, J. David, G. Brandão, E. Da Silva, L. Portugal, P. Dos Reis, A. Souza, W. Dos Santos, Box-Behnken design: An alternative for the optimization of analytical methods, Anal. Chim. Acta. 597 (2007) 179–186. doi:10.1016/j.aca.2007.07.011.

[30] G. Derringer, R. Suich, Simultaneous Optimization of Several Response Variables, J. Qual. Technol. 12 (1980) 214–219.

[31] N. Costa, J. Lourenço, Z. Pereira, Desirability function approach: A review and performance evaluation in adverse conditions, Chemom. Intell. Lab. Syst. 107 (2011) 234–244. doi:10.1016/j.chemolab.2011.04.004.

[32] W. Falco, A. Queiroz, J. Fernandes, E. Botero, E. Falcão, F. Guimarães, J. M'peko, S. Oliveira, I. Colbeck, A. Caires, Interaction between chlorophyll and silver nanoparticles: A close analysis of chlorophyll fluorescence quenching, J. Photochem. Photobiol. Chem. 299 (2015) 203–209. doi:10.1016/j.jphotochem.2014.12.001.

[33] R. Leese, E. Wehry, Corrections for Inner-Filter effects in fluorescence quenching measurements via Right-angle and front-surface illumination, Anal Chem. 50 (1978) 1193–1196.

[34] M. Puchalski, M. Morra, R. Wandruzka, Assessment of inner filter effect corrections in

fluorimetry, Fresenius J Anal Chem. 340 (1991) 341–344.

[35] M. Bezener, S. Kraber, General sequence of analysis. ANOVA output. Interpretation of R-squared., Des.-Expert. (2017). https://www.statease.com/docs/v11/contents/analysis/interpretation-of-r-squared.html (accessed April 10, 2018).

[36] M. Cuéllar, V. Pfaffen, P. Ortiz, Application of multi-factorial experimental design to successfully model and optimize inorganic chromium speciation by square wave voltammetry, J. Electroanal. Chem. 765 (2016) 37–44. doi:10.1016/j.jelechem.2015.07.050.

[37] R.R. Wilcox, Applying Contemporary Statistical Techniques, Academic Press, Burlington, 2003.

[38] Dynamic Light Scattering. Common terms defined, Malvern, 2011.

[39] Robert J. Hunter, Zeta potential in Colloid Sciences. Principles and Applications, 3rd ed., Academic Press, San Diego, 1988.

[40] N. Pacioni, M. González-Béjar, E. Alarcón, K. McGilvray, J. Scaiano, Surface plasmons control the dynamics of excited triplet states in the presence of gold nanoparticles, J. Am. Chem. Soc. 132 (2010) 6298–9. doi:10.1021/ja101925d.

Figure captions

Scheme 1. Chemical structure for GA

Fig. 1. Pareto chart. The vertical line indicates a critical t-value of 2.059.

Fig. 2. Response surfaces plots for A_{max} as a function of variables in the Box-Behnken design: (A) $AgNO_3$ and GA concentrations, (B) $AgNO_3$ concentration and reaction time and (C) GA concentration and reaction time.

Fig. 3. Response surfaces plots for λ_{max} as a function of variables in the Box-Behnken design: (A) $AgNO_3$ and GA concentrations, (B) $AgNO_3$ concentration and reaction time and (C) GA concentration and reaction time.

Fig. 4. Response surfaces plots for FWHM as a function of variables in the Box-Behnken design: (A) $AgNO_3$ and GA concentrations, (B) $AgNO_3$ concentration and reaction time and (C) GA concentration and reaction time.

Fig. 5. Absorption spectra for (a-c) three different batches of $AgNP_g^{opt}$ and (d-e) three different batches of $AgNP_g$. Solvent: water. Temperature: 25.0ºC.

Fig. 6. Histograms for four different batches of $AgNP_g^{opt}$ showing size distribution according to TEM images. Average diameters expressed in nm were: [a] 16.3 (SD = 5.6), [b] 17.0 (SD = 4.9), [c] 17.7 (SD = 6.6) and [d] 16.2 (SD = 6.1).

Scheme 1

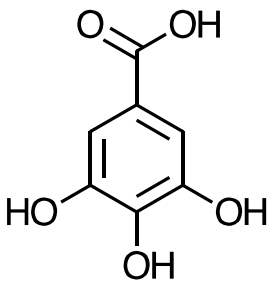

Fig. 1

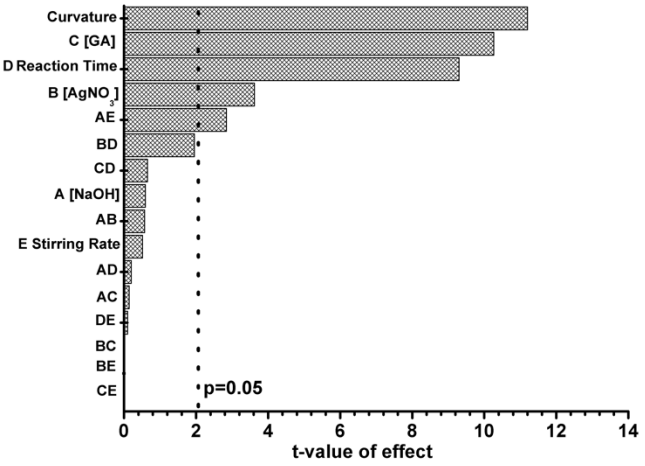

Fig. 2

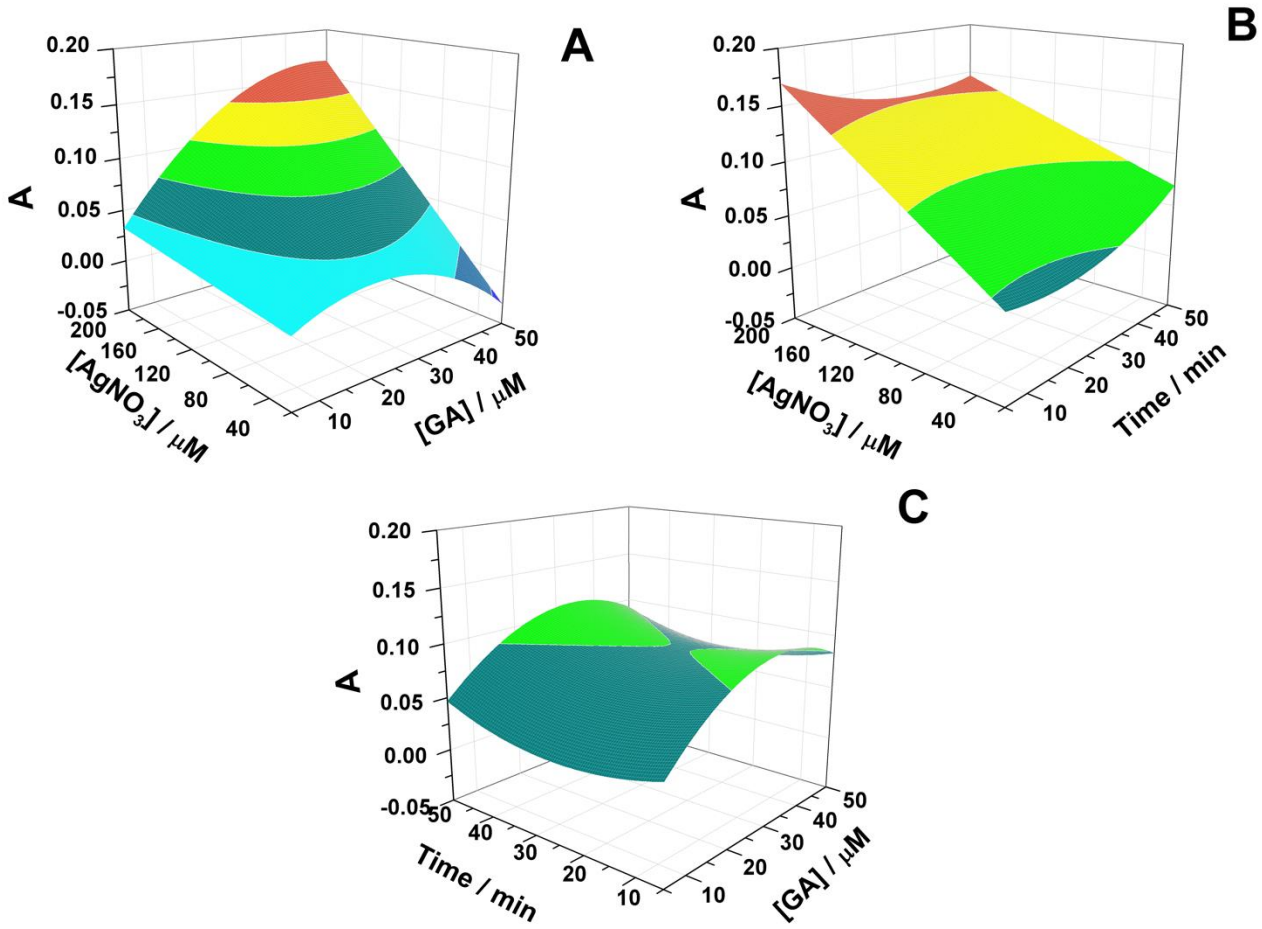

Fig. 3

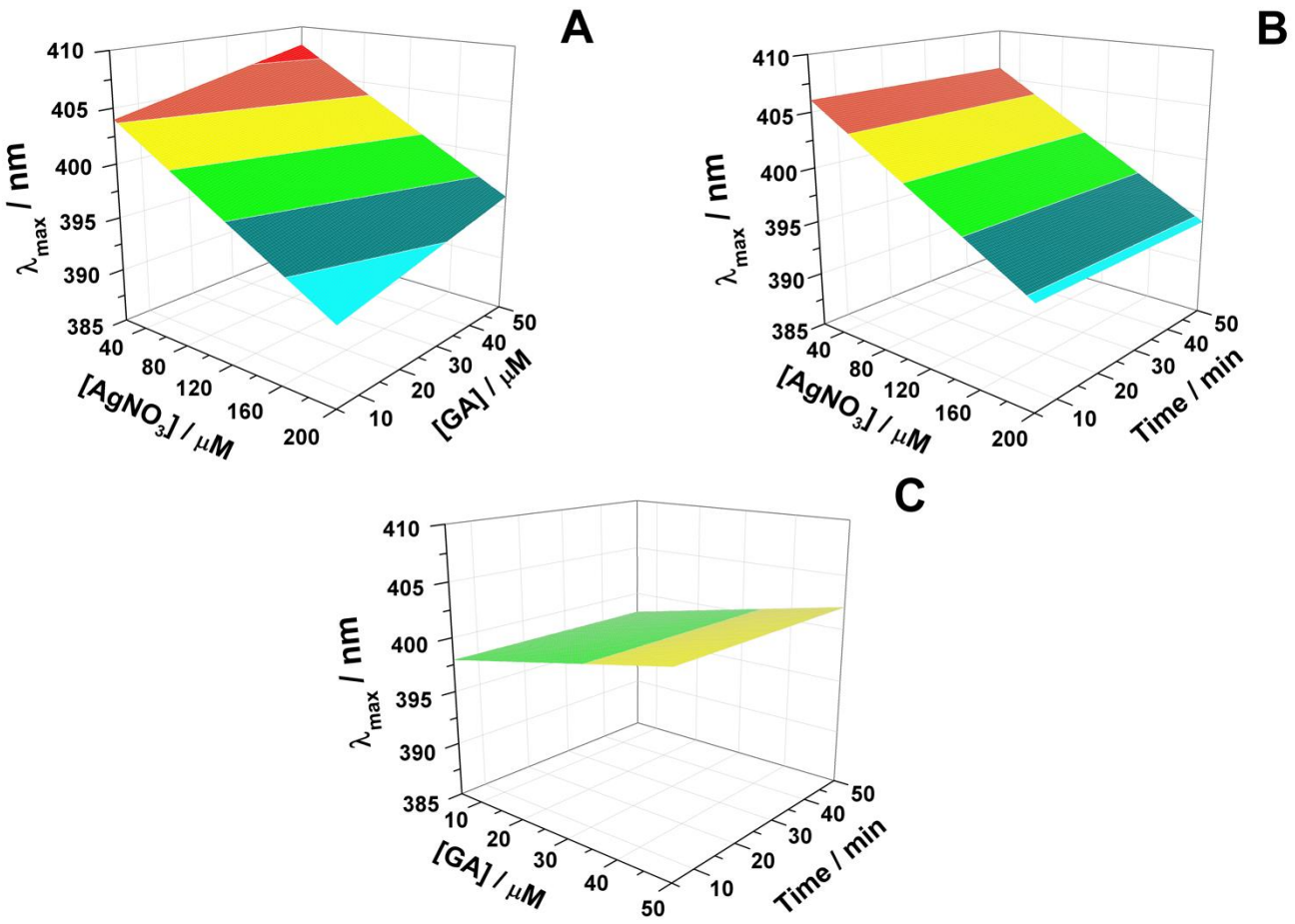

Fig. 4

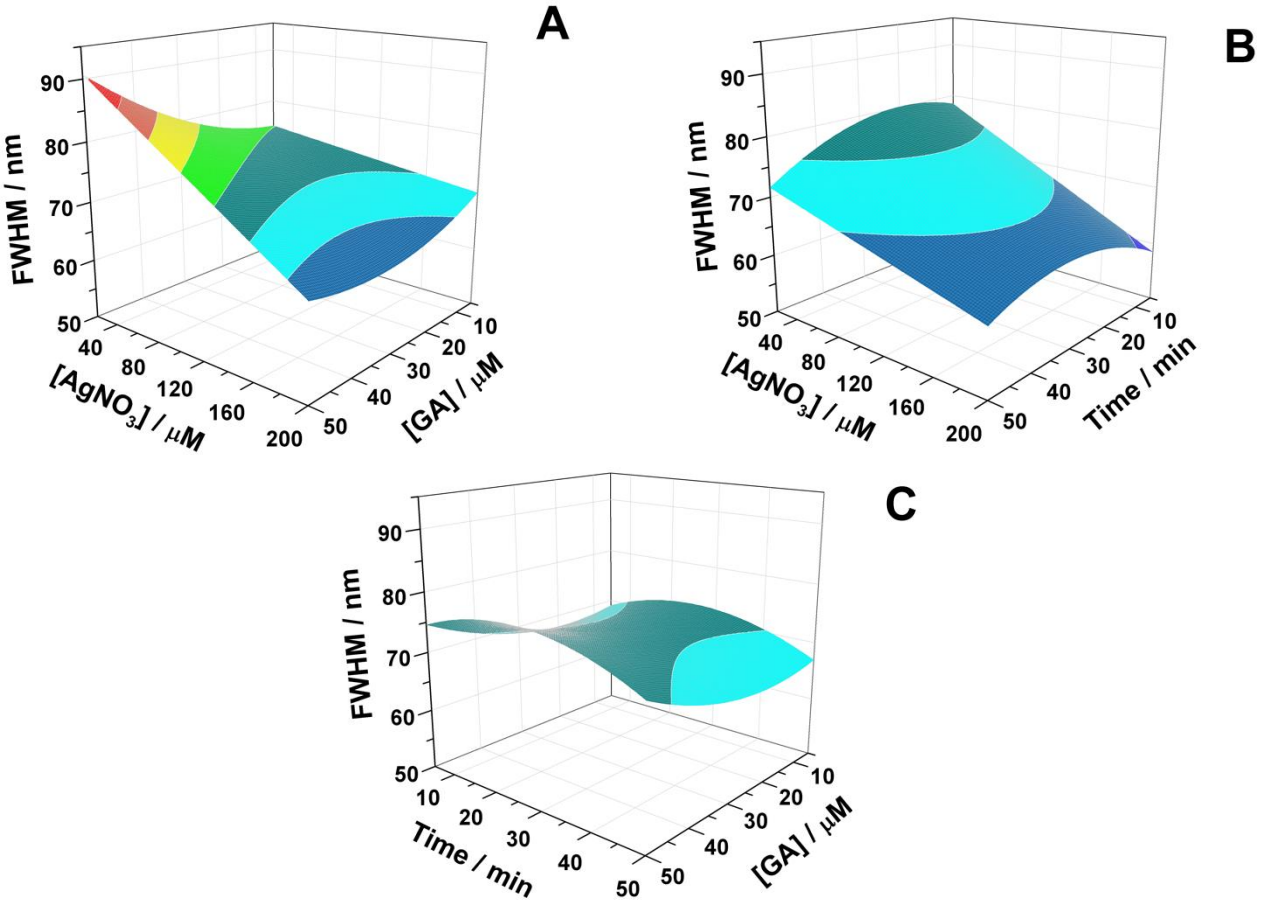

Fig. 5

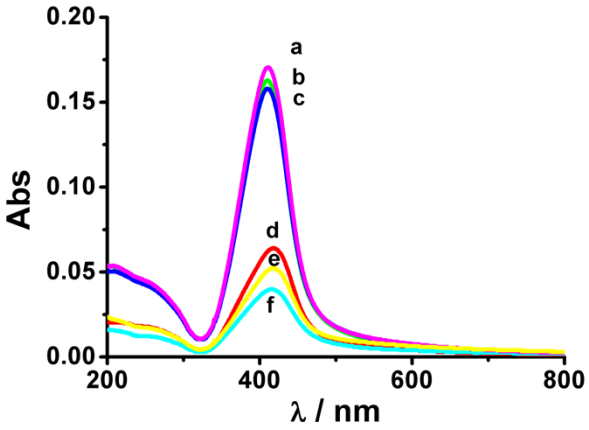

Fig. 6

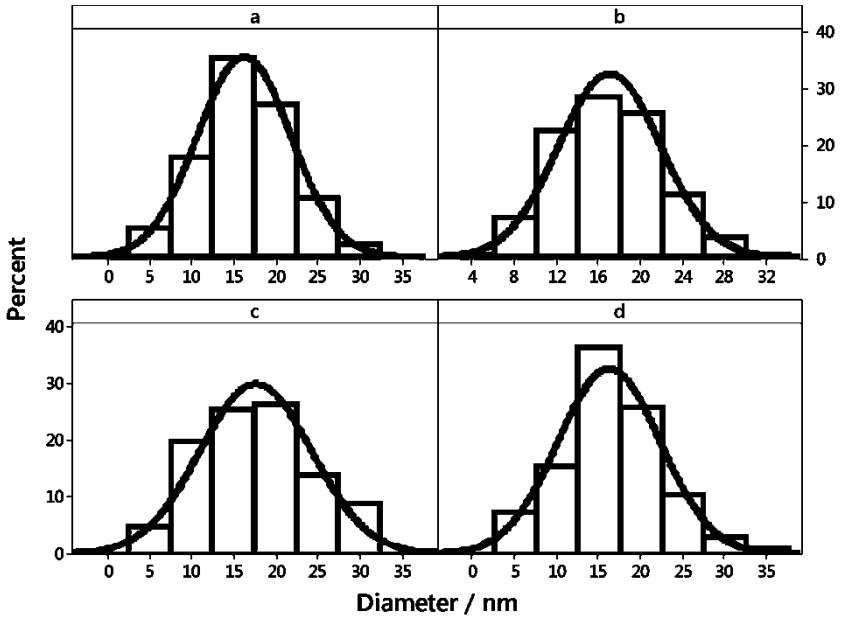

Supplementary material

Improving reproducibility between batches of silver nanoparticles using an experimental design approach.

Rodrigo Nicolás Núñez[1,2], Alicia Viviana Veglia[1,2] and Natalia Lorena Pacioni[1,2]*

[1]*Universidad Nacional de Córdoba, Facultad de Ciencias Químicas, Departamento de Química Orgánica. Haya de la Torre y Medina Allende s/n, X5000HUA, Ciudad Universitaria, Córdoba, Argentina.*

[2]*Consejo Nacional de Investigaciones Científicas y Técnicas (CONICET), INFIQC, Córdoba, Argentina. Phone: +54-351-5353867*

Corresponding author*: nataliap@fcq.unc.edu.ar*

Table S1. Analysis of Variance for 2_V^{5-1} FFD

Source of variation	Sum of squares	d.f.*	Mean square	F	p
Model	18.850	12	1.570	18.25	<0.0001
A [NaOH]	0.030	1	0.030	0.35	0.5579
B [$AgNO_3$]	1.130	1	1.130	13.09	0.0012
C [GA]	8.940	1	8.940	103.96	<0.0001
D reaction time	7.450	1	7.450	86.59	<0.0001
E stirring rate	0.023	1	0.023	0.26	0.6124
AB	0.028	1	0.028	0.33	0.5727
AC	0.001	1	0.001	0.02	0.8982
AD	0.003	1	0.003	0.04	0.8525
AE	0.700	1	0.700	8.08	0.0084
BC	0.000	0			
BD	0.330	1	0.330	3.81	0.0613
BE	0.000	0			
CD	0.036	1	0.036	0.42	0.5231
CE	0.000	0			
DE	0.001	1	0.001	0.01	0.9358
Curvature	1.920	1	1.920	125.45	<0.0001
Residual	2.320	27	0.086		
Lack of Fit	2.120	17	0.120	6.18	0.0029
Pure Error	0.200	10	0.020		
Total	21.180	40			

* d.f.: degrees of freedom

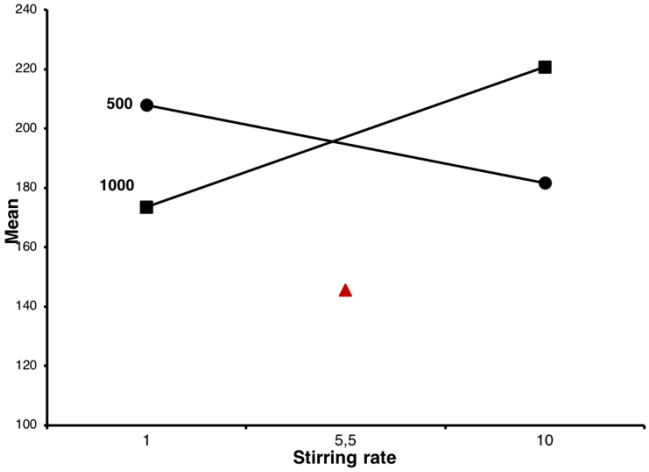

Fig. S1. Interaction plot from FFD of response (Ψ) means (10^{-8} nm^{-2}). [NaOH] in μM were (●) 500, (▲)750 and(■) 1000.

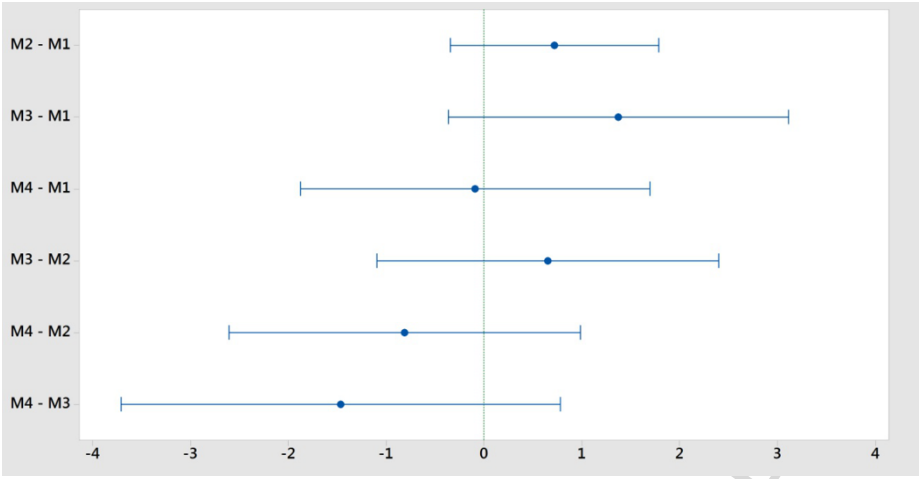

Fig. S2. Graph for the multiple comparison test using the Games-Howell method. M1, M2, M3 and M4 are the $AgNP_g^{opt}$ batches. Vertical line indicates the zero value.

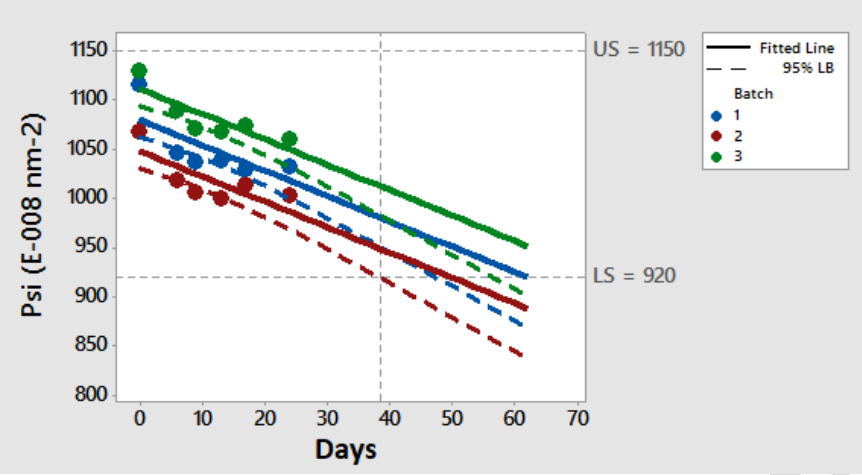

Fig. S3. Test to estimate shelf life time using three different batches of $AgNP_g^{opt}$ and monitoring the ψ response for 25 days. Upper and lower limits are indicated using horizontal lines. Vertical line indicates the predicted shelf life time.

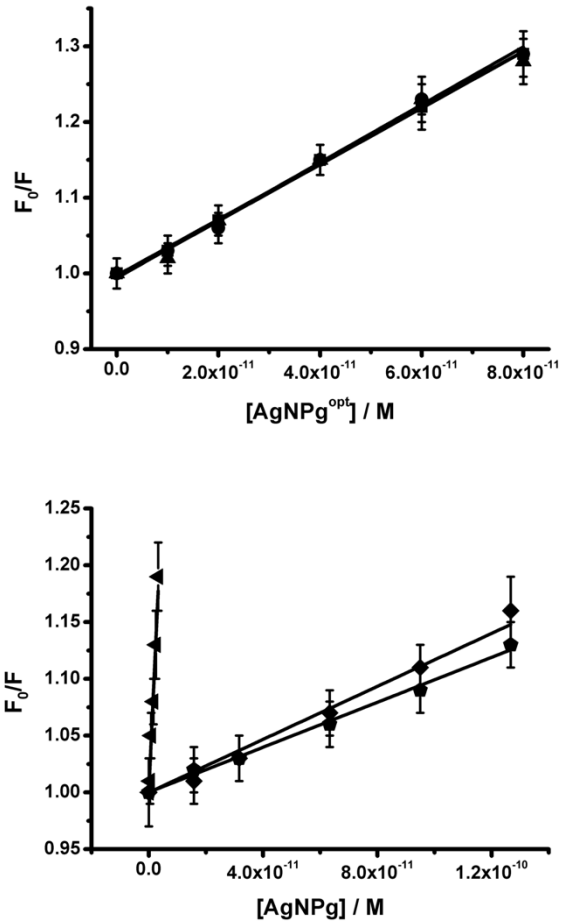

Fig. S4. Stern-Volmer plots for the fluorescence quenching of CZL by different batches synthesized under equal conditions of (*top*) $AgNP_g^{opt}$ and (*bottom*) $AgNP_g$. Solvent: 95% v/v 0.05M phosphate buffer pH 6.94, 2% v/v methanol. Temperature: 25.0 ºC. λ^{ex}: 290.0 nm.

HIGHLIGHTS

- A systematized approach to obtain reproducible batches of silver nanoparticles.
- An optimized synthesis method to produce monodisperse silver nanoparticles in high concentration using gallic acid.
- An enhanced reproducibility between nanoparticle batches in determining Stern-Volmer constants.

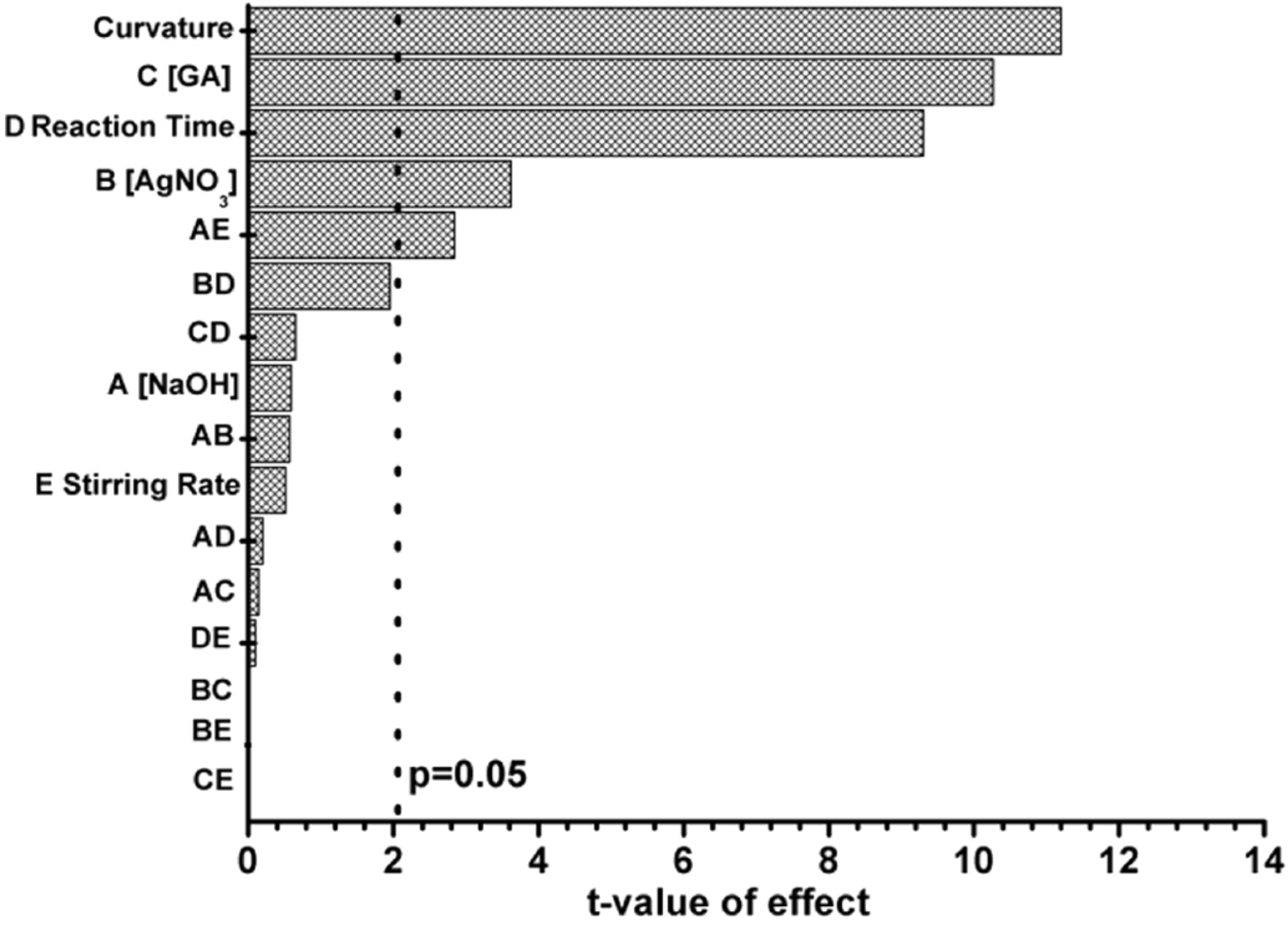
Curvature
C [GA]
D Reaction Time
B [AgNO3]
AE
BD
CD
A [NaOH]
AB
E Stirring Rate
AD
AC
DE
BC
BE
CE
p=0.05
0
2
4
6
8
10
12
14
t-value of effect

Figure 1

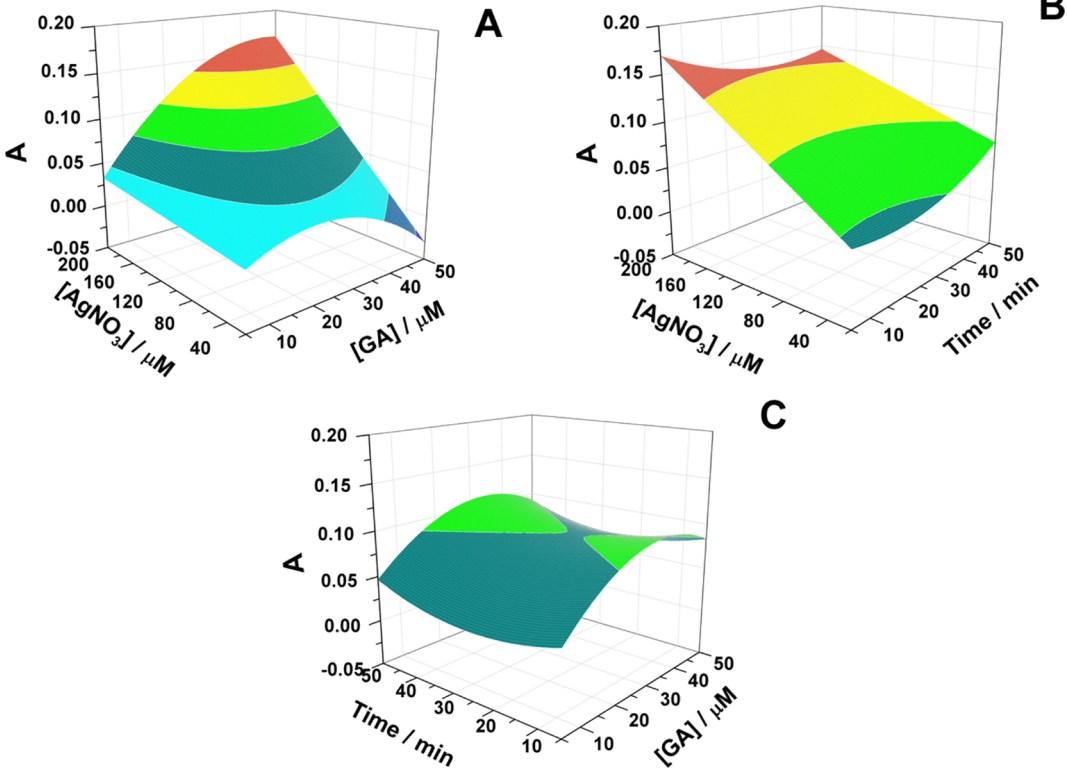
A
0.20
0.15
0.10
0.05
0.00
-0.05
A
200
160
120
80
40
[AgNO3] / μM
10
20
30
40
50
[GA] / μM
B
0.20
0.15
0.10
0.05
0.00
-0.05
A
200
160
120
80
40
[AgNO3] / μM
10
20
30
40
50
Time / min
C
0.20
0.15
0.10
0.05
0.00
-0.05
A
50
40
30
20
10
Time / min
10
20
30
40
50
[GA] / μM

Figure 2

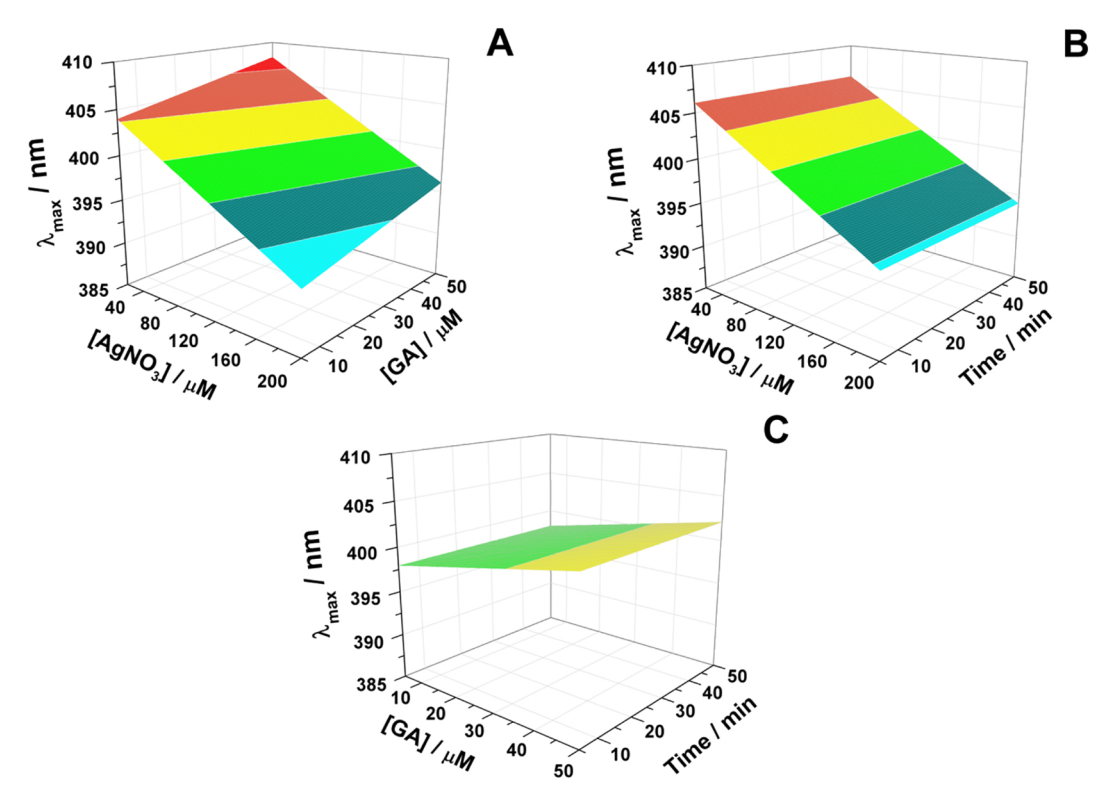
A
B
C
λ_{max} / nm
410
405
400
395
390
385
[AgNO3] / μM
40
80
120
160
200
[GA] / μM
10
20
30
40
50
Time / min

Figure 3

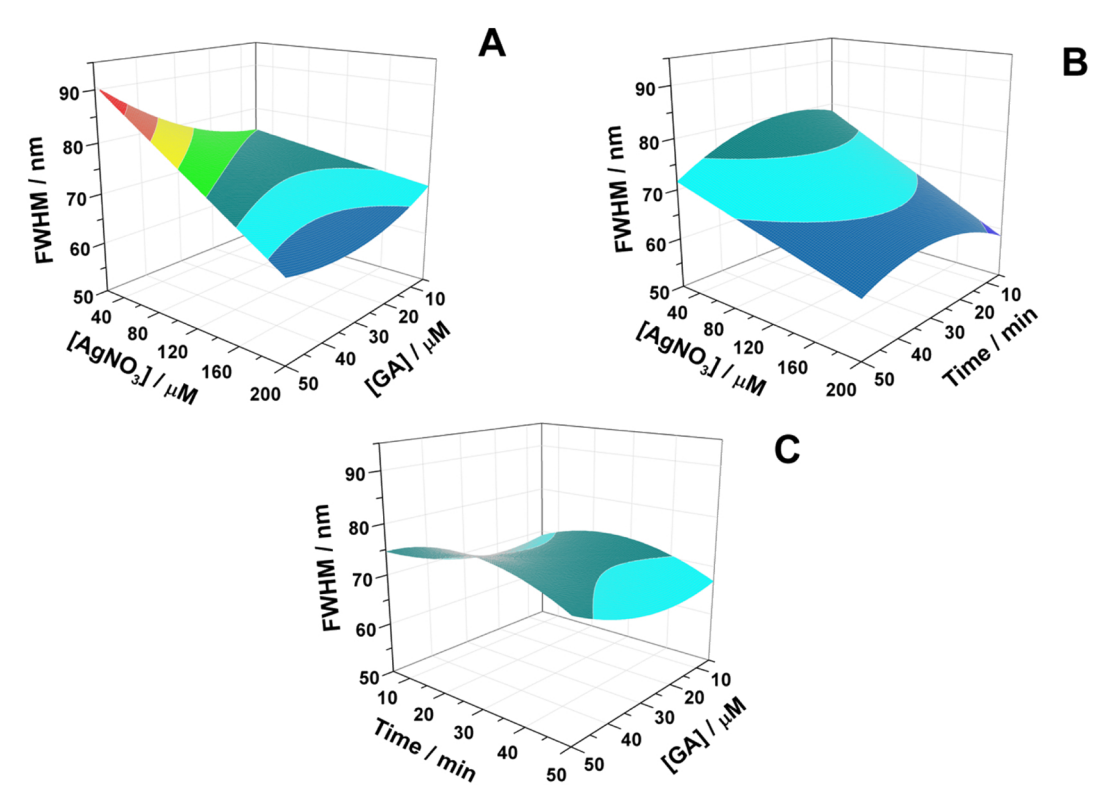
A
FWHM / nm
90
80
70
60
50
40
80
120
160
200
[AgNO3] / μM
10
20
30
40
50
[GA] / μM
B
FWHM / nm
90
80
70
60
50
40
80
120
160
200
[AgNO3] / μM
10
20
30
40
50
Time / min
C
FWHM / nm
90
80
70
60
50
10
20
30
40
50
Time / min
10
20
30
40
50
[GA] / μM

Figure 4

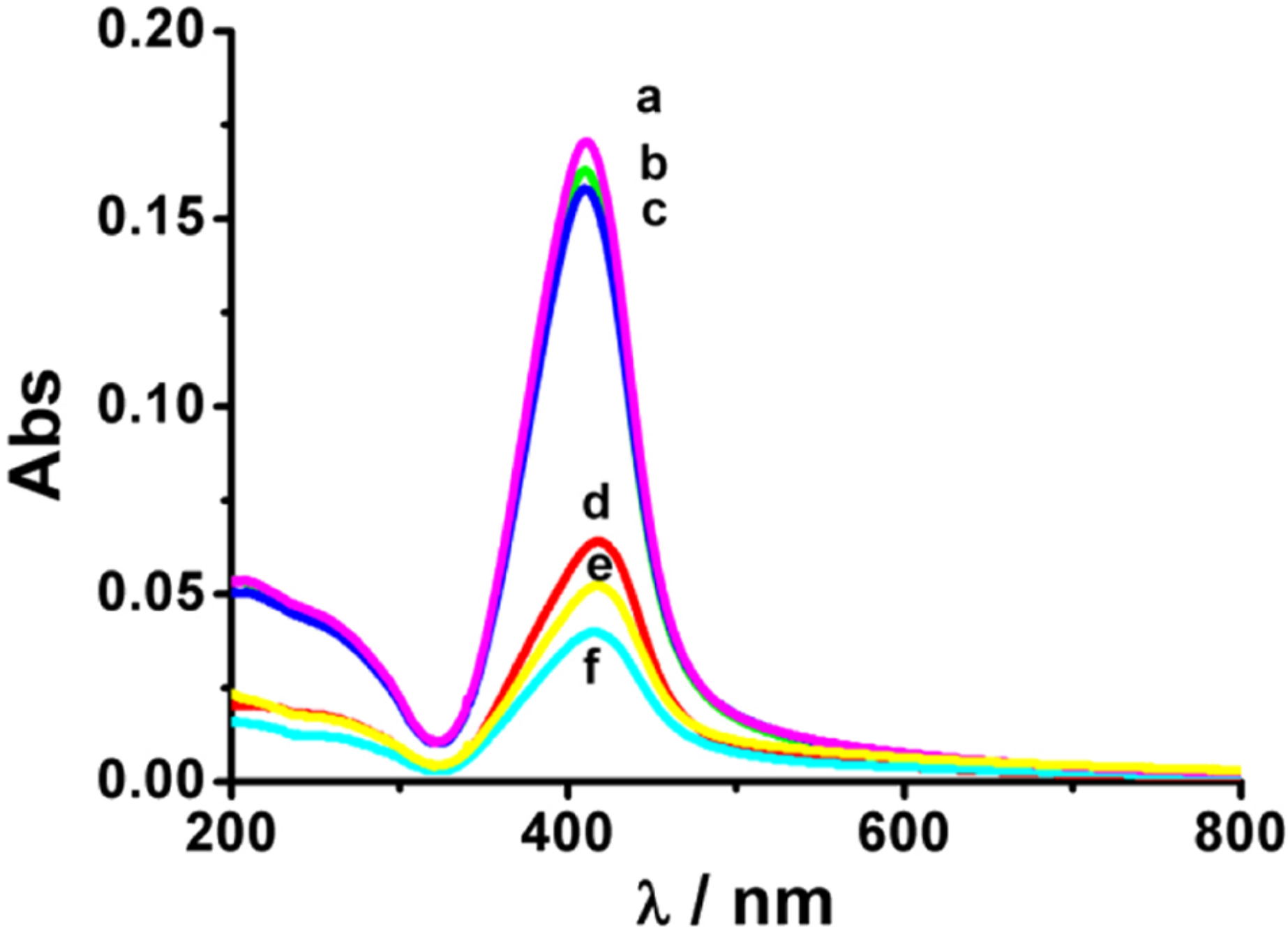

Figure 5

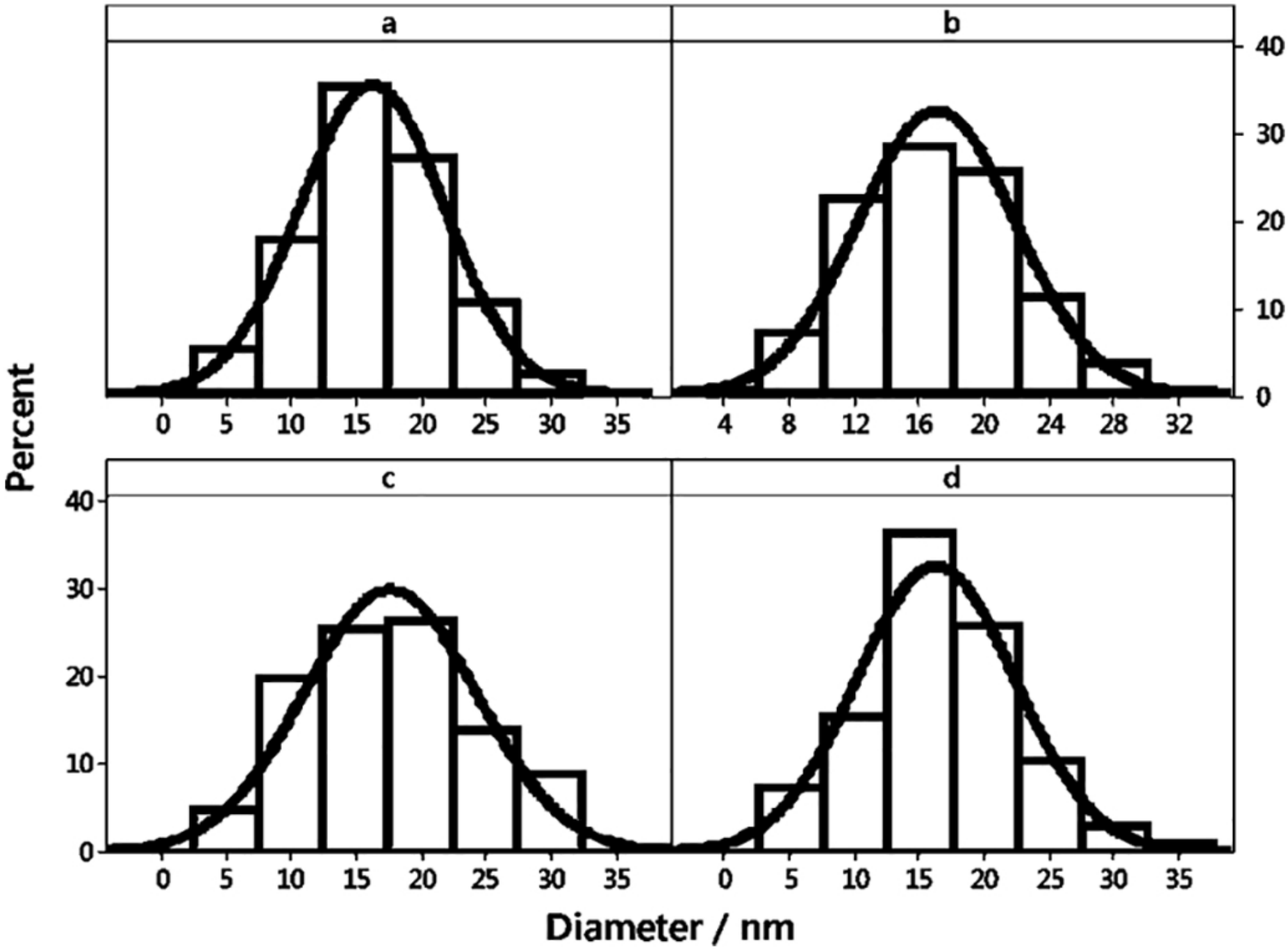
a
b
c
d
Percent
Diameter / nm
0
5
10
15
20
25
30
35
4
8
12
16
20
24
28
32
40
30
20
10
0

Figure 6

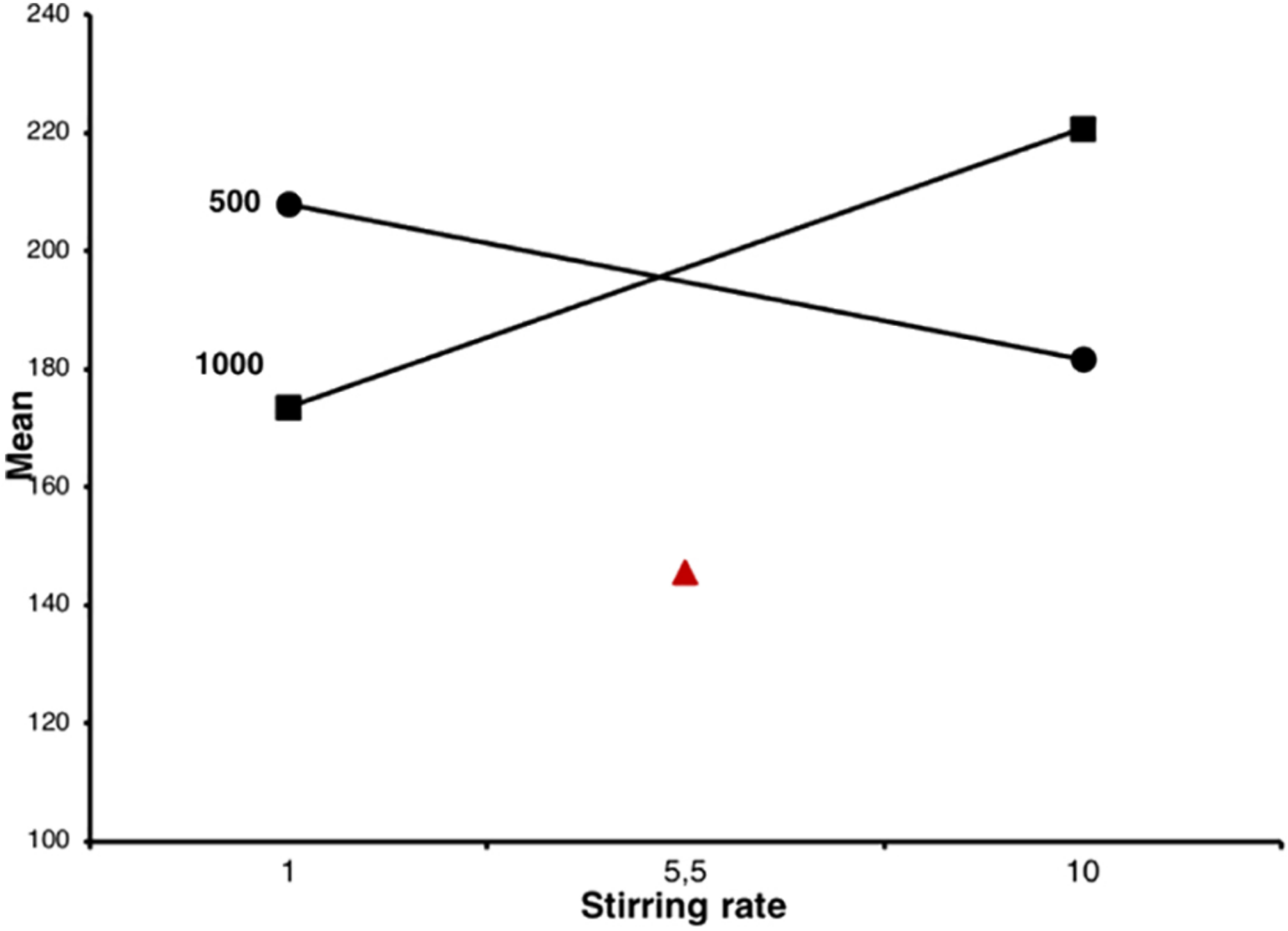
240
220
200
180
160
140
120
100
Mean
500
1000
1
5,5
10
Stirring rate

Figure 7

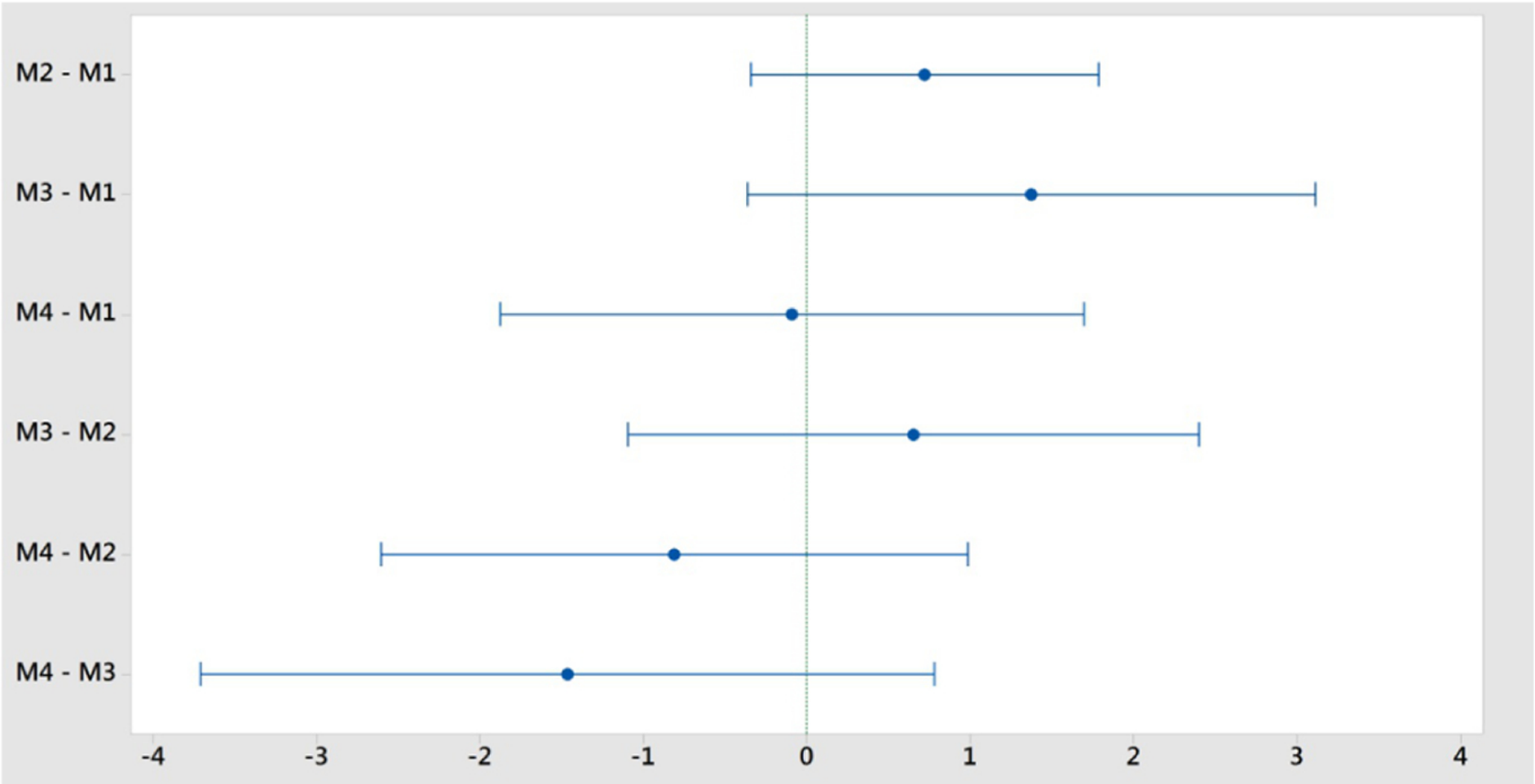

Figure 8

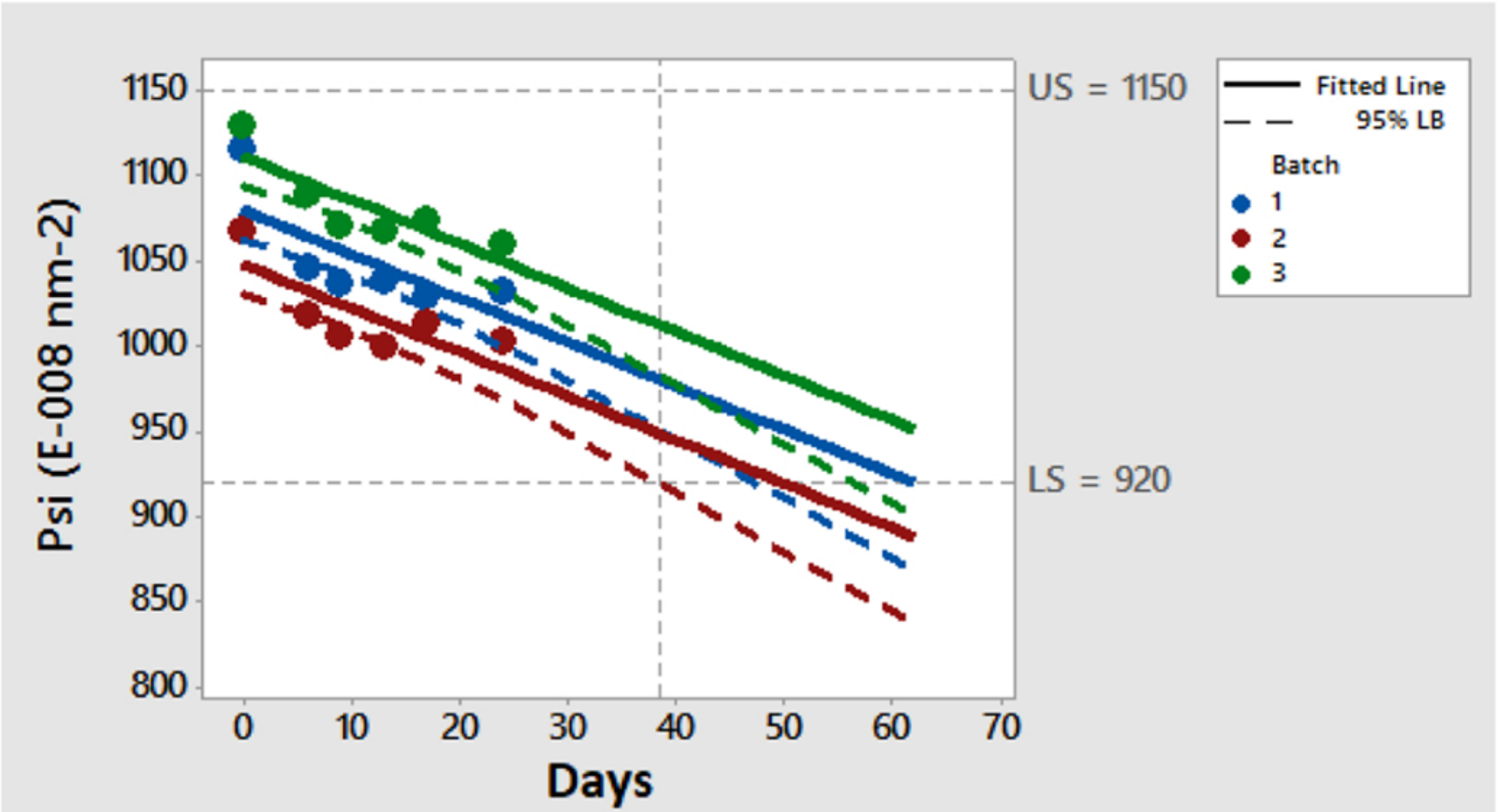
Psi (E-008 nm-2)
1150
1100
1050
1000
950
900
850
800
US = 1150
LS = 920
0
10
20
30
40
50
60
70
Days
Fitted Line
95% LB
Batch
1
2
3

Figure 9

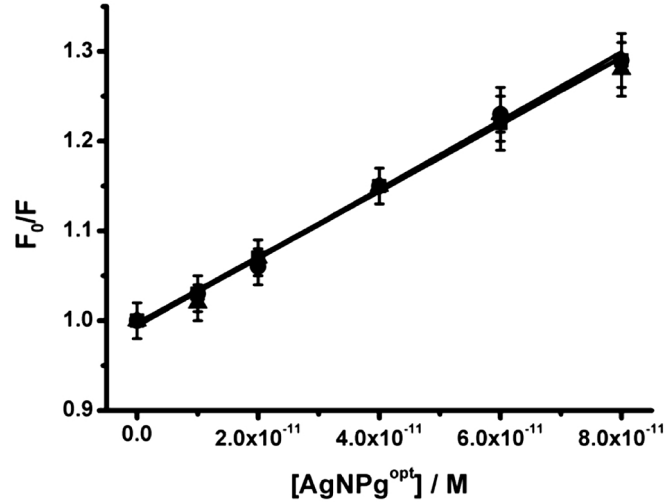
1.3
1.2
1.1
1.0
0.9
F_0/F
0.0
$2.0x10^{-11}$
$4.0x10^{-11}$
$6.0x10^{-11}$
$8.0x10^{-11}$
$[AgNPg^{opt}]$ / M

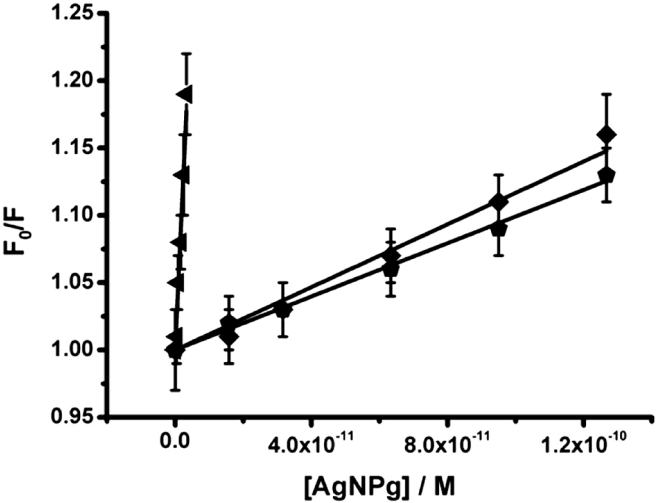
1.25
1.20
1.15
1.10
1.05
1.00
0.95
F_0/F
0.0
$4.0x10^{-11}$
$8.0x10^{-11}$
$1.2x10^{-10}$
[AgNPg] / M

Figure 10